ADVANCES IN ATMOSPHERIC SCIENCES, VOL. 22, NO. 6, 2005, 852–864

Tropical Precipitation Estimated by GPCP and TRMM PR Observations

LI Rui (李 锐) and FU Yunfei* (傅云飞)

School of Earth and Space Sciences, University of Science and Technology of China, Hefei 230026

(Received 31 January 2004; revised 20 May 2005)

ABSTRACT

In this study, tropical monthly mean precipitation estimated by the latest Global Precipitation Climatology Project (GPCP) version 2 dataset and Tropical Rainfall Measurement Mission Precipitation Radar (TRMM PR) are compared in temporal and spatial scales in order to comprehend tropical rainfall climatologically. Reasons for the rainfall differences derived from both datasets are discussed. Results show that GPCP and TRMM PR datasets present similar distribution patterns over the Tropics but with some differences in amplitude and location. Generally, the average difference over the ocean of about 0.5 mm d^{-1} is larger than that of about 0.1 mm d^{-1} over land. Results also show that GPCP tends to underestimate the monthly precipitation over the land region with sparse rain gauges in contrast to regions with a higher density of rain gauge stations. A Probability Distribution Function (PDF) analysis indicates that the GPCP rain rate at its maximum PDF is generally consistent with the TRMM PR rain rate as the latter is less than 8 mm d^{-1}. When the TRMM PR rain rate is greater than 8 mm d^{-1}, the GPCP rain rate at its maximum PDF is less by at least 1 mm d^{-1}compared to TRMM PR estimates. Results also show an absolute bias of less than 1 mm d^{-1} between the two datasets when the rain rate is less than 10 mm d^{-1}. A large relative bias of the two datasets occurs at weak and heavy rain rates.

Key words: GPCP, TRMM PR, precipitation

1. Introduction

Tropical rainfall is critical to regulating the global hydrological cycle, for which it comprises more than two thirds of the global precipitation. The latent heat release associated with the tropical rainfall contributes approximately three fourths of the energy that drives the atmospheric circulation (Kummerow et al., 2000). However, there are still many uncertainties regarding the tropical precipitation in the measurements and model simulations due to its large temporal and spatial variations.

Intercomparisons of precipitation datasets (Barret et al., 1994; Ebert, 1996; Smith et al., 1998; Cruber et al., 2000; Soden, 2000; Adler et al., 2001; New et al., 2001; etc.) have been made for recommendations on accuracy and usefulness for a variety of applications, including global model output validation, climate change monitoring and diagnostics. In the third Precipitation Intercomparison Project (PIP3, Adler et al., 2001), 31 precipitation products were compared. The project revealed a very large difference in rainfall estimations. Even in zonal averages, annual total precipitation displays a factor of 2 to 3 between the smallest and largest values, depending on the latitude. The model-based [such as ECMWF (European Centre for Medium-Range Weather Forecasts), NCEP (National Centers for Environmental Prediction), AMIP (Atmospheric Model Intercomparison Project) and GEOS (Goddard Earth Observing System) model], precipitation distributions are shown to do significantly poorer than the observational ones in the Tropics. Additionally, since each product may hold advantages in certain locations or situations, it is difficult to decide which is best in terms of a monthly precipitation total over most of the globe.

Among precipitation datasets, the GPCP (Global Precipitation Climatology Project) data developed by Huffman and Adler (Huffman et al., 1997; Adler et al., 2003) has become very spatial and useful in unveiling the temporal and special distribution of tropical precipitation. GPCP merges precipitation datasets involving sequential measurements of rain gauges from

*E-mail: fyf@ustc.edu.cn

Table 1. Satellite remote-sensing precipitation datasets used by GPCP.

Sensor	Coverage	Dataset	Reference
Infrared radiation	40°N–40°S	GPI	Arkin and Meisner, 1987
Outgoing longwave radiance	90°N–90°S	OPI	Xie and Arkin, 1998
Passive microwave emission	60°N–60°S	SSM/I Emission	Wilheit et al., 1991
Passive microwave scattering	60°N–60°S	SSM/I Scattering	Ferraro et al., 1996
			Ferraro and Marks, 1995
Others*	90°N–90°S	TOVS	Susskind et al., 1997
Active passive microwave		Not Used	

*Include: cloud-top pressure, fractional cloud cover, and relative humidity profile.

the GPCC (Global Precipitation Climatology Centre, Rudolf, 1993; Rudolf et al., 1994) and various satellite-based (see Table 1) observations. However, differences between GPCP and TRMM (Tropical Rainfall Measurement Mission) PR (Precipitation Radar) have not been addressed in detail.

TRMM PR is the first active satellite microwave instrument for measuring three-dimensional structures of rainfall over the Tropics and subtropics (Simpson et al., 1998; Kummerow et al., 2000). Its products have been applied to exposing characteristics of precipitation profiles and their effects on microwave brightness temperatures, rainfall structures in mesoscale convective systems, rainfall retrieval algorithm improvements and cross calibration among rainfall observations (Adler et al., 2000; Fu and Liu, 2001, 2003; Liu and Fu, 2001; Petersen and Rutledge, 2001; Kummerow et al., 2001, 2004; Berg et al., 2002; Fu et al., 2003a, 2003b; Zheng et al., 2004).

In this study, rainfall differences derived from GPCP and TRMM PR over the Tropics on the monthly scale are compared for the period from 1998 to 2002 in order to comprehend uncertainties of both rainfall datasets and their reasons. The relations between the differences between both datasets and the precipitation intensity are presented as a reference for the cross correction of both datasets.

2. Data

The GPCP, designated by the WMO (World Meteorological Organization)/WCRP (World Climate Research Programme)/GEWEX (Global Energy and Water Cycle Experiment), introduces a new dataset, version 2, of precipitation with a horizontal resolution of 2.5° × 2.5° on a monthly basis, which is combined with satellite-gauge precipitation estimates over the globe for a long period (Huffman et al., 1997; Adler et al., 2003). There are 12 techniques, or algorithms, in the new dataset, viz. SSM/I (Special Sensor Microwave/Imager) emission (SSM/I E), SSM/I scattering (SSM/I S), SSM/I composite, TOVS (the TIROS Operational Vertical Sounder), SSMI/TOVS composite, OPI (OLR Precipitation Index), GPI (GOES Precipitation Index), AGPI (Adjusted GPI), multisatellite, GHCN (Global Historical Climate Network) and CAMS (Climate Assessment and Monitoring System) rain gauges, GPCC rain gauges, and satellite gauges. For example, the SSM/I E algorithm applied is the Wilheit et al. (1991) iterative histogram approach to retrieving precipitation from emission signals in the 19-GHz SSM/I channel, which infers the quantity of liquid water in a column from the increased low-frequency observed microwave brightness temperatures. Greater amounts of liquid water in the column tend to correlate with greater surface precipitation. This technique works well over the ocean where the surface emissivity is low and uniform. Over land, however, the emissivity is near unity and extremely heterogeneous, making the scattering algorithm the only choice. The scattering algorithm applied is based on the Grody (1991) Scattering Index (SI), supplemented by the Weng and Grody (1994) emission technique in oceanic areas, which infers the quantity of hydrometeor ice in a column from the depressions in the high-frequency 85-GHz channel brightness temperatures. More ice aloft typically implies more surface precipitation. This relationship is physically less direct than in the emission technique, but it works equally well over land and ocean whenever deep convection is important.

The GPCC rain gauge precipitation product is produced by the Global Precipitation Climatology Centre (Rudolf, 1993). Rain gauge reports are archived from approximately 6700 stations around the globe, both from Global Telecommunications Network reports, and from other world-wide or national data collections. An extensive quality-control system is run, featuring an automated step and then a manual step

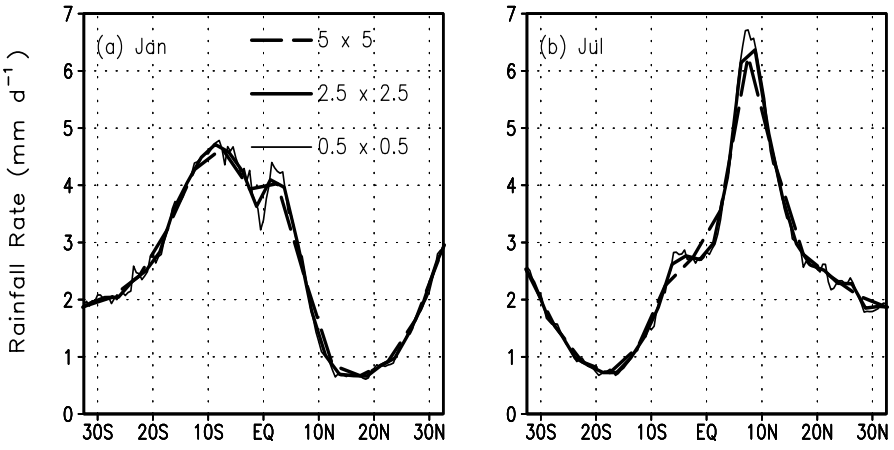

Fig. 1. Zonal mean rainfall rate of TRMM PR over the Tropics in three different horizontal resolutions. $0.5^\circ \times 0.5^\circ$, $2.5^\circ \times 2.5^\circ$, and $5^\circ \times 5^\circ$, in (a) January and (b) July averaged from 1998 to 2002.

designed to retain legitimate extreme events that characterize precipitation. For component contrast and analysis in our study, the SSM/I E estimated dataset from 1998 to 2002 is used over the tropical oceans and the GPCC dataset is used over land. Both are the main input sources of GPCP over ocean and land.

The TRMM satellite, flying at 350 km altitude (regulated to 400 km after 7 August 2001), is a non-synchronous satellite with an approximate inclination angle of 35°. Its orbital period is around 91.6 minutes and there are about 16 orbits between 38°S and 38°N each day. The TRMM PR (Iguchi and Meneghini, 1994) scanning width of about 220 km measures the rainfall rate from the earth surface to 20 km altitude with a horizontal resolution of 4.3 km (at nadir) and a vertical resolution of 0.25 km (Kummerow et al., 1998). As a result, the TRMM PR provides a high spatial resolution, the greatest information content, the best vertical resolution (80 levels), and the most directly-measured surface rainfall estimates for many applications. In our previous studies (Liu and Fu, 2001; Fu and Liu, 2001, 2003; Fu et al., 2003) and others (Shin et al., 2001), the vertical structures and their variability of both convective and stratiform precipitation types over the Tropics and Asia have been studied using TRMM standard data. In this paper, to fit the grid resolution of GPCP, the monthly averaged surface rainfall rate data with a grid resolution of $2.5^\circ \times 2.5^\circ$, which is derived from the daily gridded surface rainfall data with a horizontal resolution of $0.5^\circ \times 0.5^\circ$ calculated from the TRMM PR standard data 2A25, is used in the comparison with GPCP.

To confirm concisely the effect of grid resolution on the monthly averaged surface rainfall rate, the zonal mean rainfall rates of TRMM PR over the Tropics in January and July, averaged from 1998 to 2002 in three different horizontal resolutions ($0.5^\circ \times 0.5^\circ$, $2.5^\circ \times 2.5^\circ$, and $5^\circ \times 5^\circ$) are compared in Fig. 1, which indicates a roughly similar profile of the zonal mean rainfall rate in the three horizontal resolutions irrespective of the month. However, detailed differences can be found in the figure. The zonal mean rainfall rate profile obtained from the $0.5^\circ \times 0.5^\circ$ dataset shows non-smooth fluctuations, especially relatively large amplitude variations between 10°S and 10°N, in contrast to the smooth profiles derived from the other two resolution datasets. Another difference clearly indicates in July that there are two peaks in the zonal mean rainfall rate profile next to the equator by the 0.5° and 2.5° data, but only one peak in the 5° data. Furthermore, Fig. 1 also shows a very close similarity between the two relatively-fine-grid datasets, which may explain why the monthly rainfall rate data are supplied in the $2.5^\circ \times 2.5^\circ$ grid resolution in most circumstances.

3. Spatial pattern

The horizontal distribution of monthly mean precipitation estimated by GPCP and PR from 1998 to 2002 is shown in Figs. 2a and 2b. A similar pattern of rainfall over the Tropics is presented by both datasets, i.e. the highest precipitation areas are located in the monsoon region from the Indian Ocean to southern Asia, in the Intertropical Convergence Zone (ITCZ) from the Pacific Ocean to the Atlantic Ocean, in the Southern Pacific Convergence Zone (SPCZ) over the southwestern Pacific Ocean, and in the regions of south America and tropical Africa. Figure 2c shows the distributions of absolute differences between Figs. 2a and 2b. A t-test of the significance of the difference in each

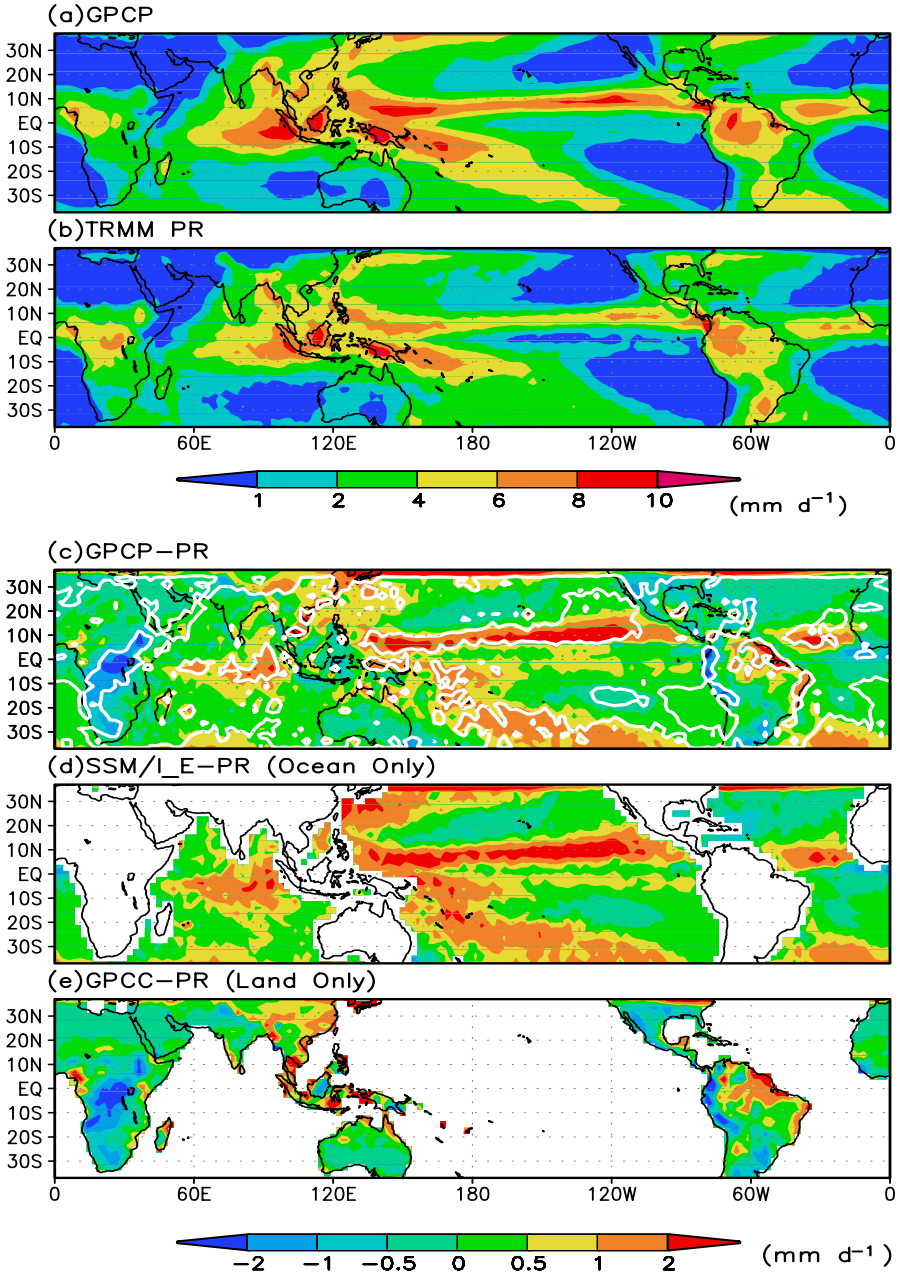

Fig. 2. Precipitation distributions averaged from 1998 to 2002 by (a) GPCP and (b) TRMM PR, and the distributions of the absolute difference between (c) GPCP and TRMM PR, (d) between SSM/I E and TRMM PR, and (e) between GPCC and TRMM PR.

box is performed to the extrude the significant differences at the 95% confidence level between both mean precipitations, which are enclosed by the white lines in Fig. 2c.

It is clear that the mean precipitation estimate by GPCP is higher than that of TRMM PR almost everywhere over the tropical oceans (0.5 mm d^{-1} on average). The areas where a significant difference exists correspond to the aforementioned heavy precipitation zones in the tropical oceans and their vicinity. For example, the most significant absolute difference of greater than 2 mm d^{-1} can be found in the Pacific ITCZ and its northern brim. So, it is easy to conclude that the estimated precipitation intensity by GPCP is larger than that by TRMM PR.

Since the main data source of GPCP precipitation

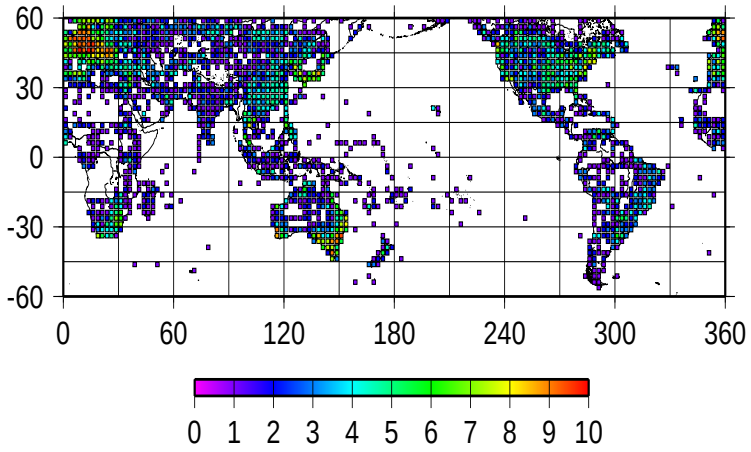

Fig. 3. The distribution of GPCC stations.

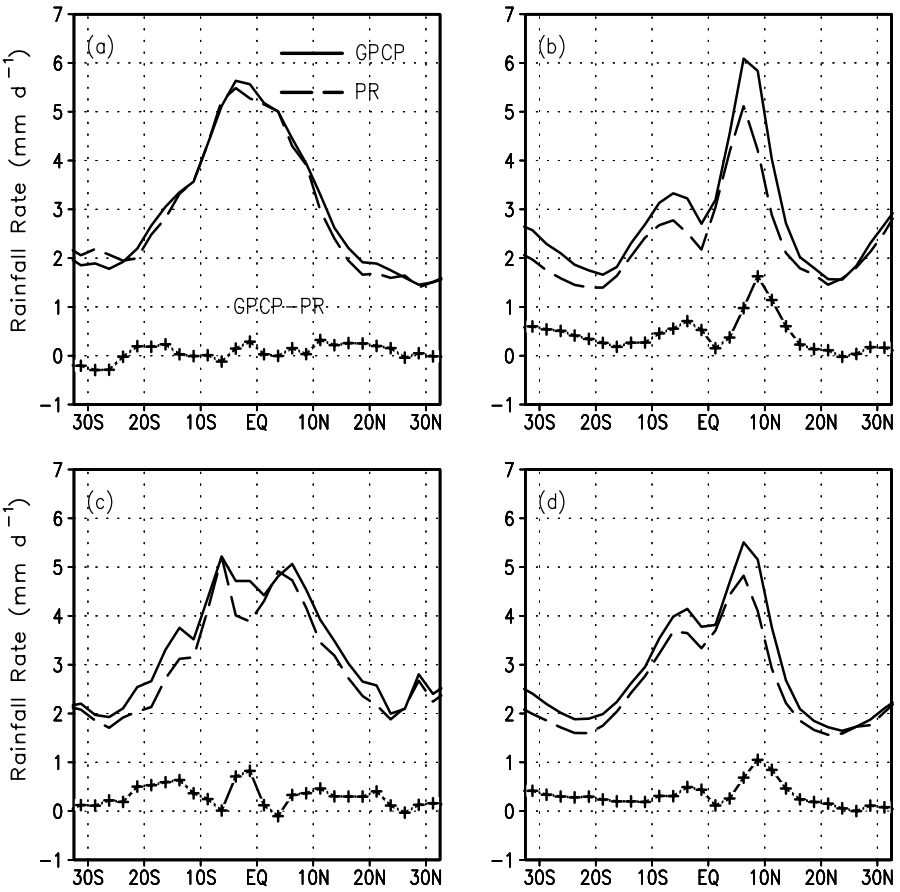

Fig. 4. Zonal-average profiles of mean precipitation of GPCP (solid line) and TRMM PR (dashed line) and their difference (crosshair symbols) over (a) land, (b) ocean, (c) coast, and (d) all. (units: mm d^{-1}).

over the 40°S–40°N oceanic region comes from SSM/I E, the horizontal distribution of the difference between SSM/I E precipitation and TRMM PR precipitation is also presented in Fig. 2d to show how large the contribution of SSM/I E is to GPCP. Compared with Fig. 2c in oceanic regions, it is obvious that the differences

in amplitude and distribution between SSM/I E and TRMM PR are very close to those over the ocean between GPCP and TRMM PR precipitation. Therefore, it is believed that the difference between GPCP and PR precipitation over the ocean is largely a result of the discrepancies between the TRMM PR and SSM/I E estimates. It also indicates the rainfall overestimated by SSM/I, which is similar to the results of TMI (Kummerow et al., 1998) rainfall retrievals by Kummerow et al. (2000) and Shin et al. (2001).

The difference between GPCP and TRMM PR precipitation estimates over tropical land is generally smaller than that over the ocean in Fig. 2c. On average, the difference is about 0.1 mm d^{-1}. Since GPCP precipitation estimates over land are mainly generated by rain gauges, the above result indicates that the TRMM PR rainfall estimates over tropical land are more consistent with the observations of the rain gauges, which is confirmed by comparing Fig. 2e (plotted by using GPCC data) with Fig. 2c over land (except for the Indonesia Islands maritime regions). Generally, the difference between GPCP and TRMM PR over land is mainly positive, but significant negative differences do occur in a few regions. Through checking the distribution of GPCC rain gauge stations (Fig. 3), it is revealed that the negative differences between GPCP precipitation and TRMM PR precipitation are usually located in areas with sparse or even no rain gauge stations, such as in Congo, Angola, Namibia in Africa, the Pacific coastal regions of Ecuador and Peru, and the Himalayas in Eurasia. On the contrary, in regions with dense rain gauge stations, positive differences dominate. Thus, the difference between GPCP and TRMM PR precipitation over land is largely the consequence of rain gauge numbers. In regions where rain gauges are sparsely laid, GPCP tends to underestimate precipitation there, whereas in regions where they are densely arrayed, TRMM PR precipitation is less than the observation of the gauges.

In addition, significant differences between GPCP and TRMM PR precipitation are also found in coastal areas. Gruber et al. (2000) found similar phenomena when comparing the GPCP and CMAP (CPC Merged Analysis of Precipitation) (Xie and Arkin, 1997) datasets. On the Atlantic coast of southern Africa (30°–15°S) and the Pacific coast of South America, GPCP rainfall is lower than TRMM PR estimates. On the other hand, on the Atlantic coast of South America and the coastline areas of mid latitudinal Asia, significant positive differences are obvious between the two estimates. The combinatory techniques of GPCP in the coastal areas could be the main cause of this phenomenon.

Figure 4 presents the zonal-average GPCP and TRMM PR precipitations and their difference over land, ocean, coast, and all surfaces. GPCP and TRMM PR unanimously reveal a single peak pattern at about 4°S over tropical land (Fig. 4a). Between 35°S and 35°N, both datasets show little difference less than 0.1 mm d^{-1}. Over the ocean, both datasets show a two-peak pattern with the peaks located at about 6°S and 6°N, respectively (Fig. 4b). The peak value in the Northern Hemisphere corresponds to the ITCZ position while the peak in the Southern Hemisphere to the SPCZ position. Comparing with that over land, the difference between GPCP and TRMM PR over the ocean is distinctly greater. It is worth noticing that the difference between the two datasets over the ocean also shows two peaks, and in the location where the zonal-average precipitation is greater, the difference is more significant as well. However, Fig. 4b also shows about one grid (2.5°) discrepancy between the peaks displayed by both averaged datasets and both differences. The latter's peaks are located at about 4°S and 9°N, respectively. This is attributed to the fact that the longitudinally extended precipitation zones, such as the ITCZ and SPCZ, etc., as estimated by GPCP are significantly larger than that estimated by TRMM PR. In coastal regions, precipitation estimated by both datasets also assumes a two-peak pattern with peaks symmetrically located at about 5°S and 5°N, respectively (Fig. 4c). However, the maximum difference amplitude between both datasets in the coastal regions is comparatively smaller than that over ocean.

As a summary for zonal averaged rainfall over the whole Tropics, patterns generated by both datasets and their differences are very close to those displayed over the tropical ocean since most tropical areas are covered by the sea (Fig. 4d).

4. Temporal variability

In order to reveal rainfall differences estimated by GPCP and TRMM PR on the seasonal scale, the seasonal cycle of precipitation over land and ocean is plotted by using both datasets as well as their both difference in the four latitudinal zones, from 15°N to 37°N, 0° to 15°N, 15°S to 0°, and 15°S to 37°S, respectively, in Fig. 5. Seasonal mean differences of rainfall from winter (DJF, December) to fall (SON) between GPCP and TRMM PR in each zone are listed in Table 2. It reveals a positive departure of GPCP from TRMM PR over the ocean regardless of season. The maximum departure of both datasets over the ocean appears in the zone from 0° to 15°N in all four seasons, which results in 0.8 mm d^{-1} in annual mean departure. In the other three zones, the seasonal mean departures are smaller than 0.65 mm d^{-1}, and the annual departures smaller

Table 2. Seasonal departures of precipitation between GPCP and TRMM PR.

		Departure (GPCP–PR, mm d^{-1})					
Background	Region	DJF	MAM	JJA	SON	Annual	SD
Land	15°–37°N	0.11	−0.07	0.48	0.31	0.21	0.24
	0°–15°N	0.31	0.16	0.04	0.03	0.13	0.13
	0°–15°S	0.41	0.30	−0.08	−0.38	0.06	0.36
	15°–37°S	0.15	0.09	0.06	−0.39	−0.02	0.25
Ocean	15°–37°N	0.15	0.32	0.32	0.48	0.31	0.13
	0°–15°N	0.72	0.66	0.98	0.83	0.80	0.14
	0°–15°S	0.61	0.56	0.29	0.37	0.46	0.15
	15°–37°S	0.58	0.49	0.30	0.46	0.46	0.12

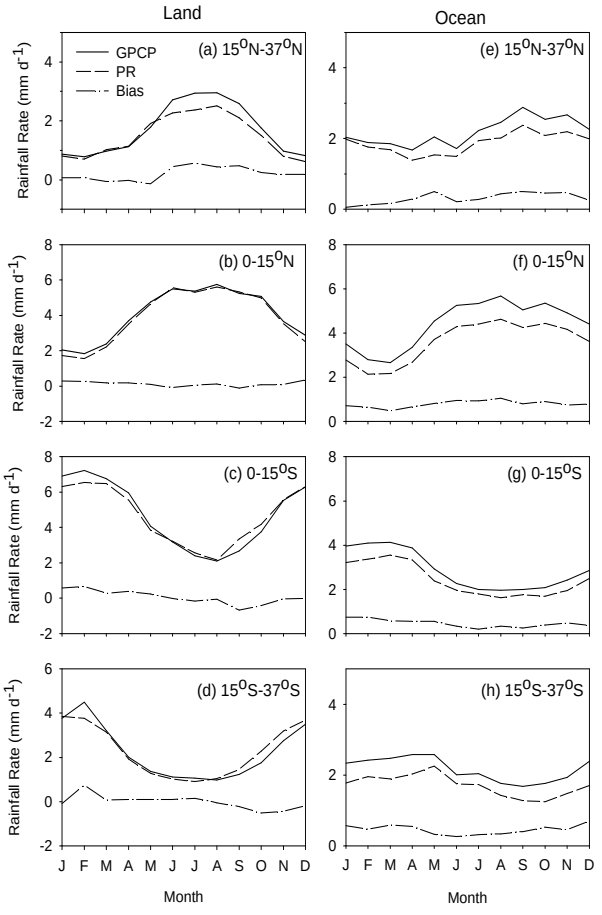

Fig. 5. Seasonal cycle of precipitation derived from GPCP and TRMM PR, and their departures over land (a, b, c, d) and ocean (e, f, g, h) in four latitudinal zones. (units: mm d^{-1}).

than 0.5 mm d^{-1}. Generally, departures over the ocean show less seasonal variability. Over land, the seasonal departures show both positive and negative values except in winter and the zone from 0° to 15°N, which means relatively large seasonal variability of the departures over land. The annual departure over land is smaller than 0.4 mm d^{-1}. So, if comparing departures between land and ocean, it is remarkable that the departure values of the latter are greater that the former regardless of zone or season. This implies a better retrieval of precipitation by GPCP over land than over the ocean. On the other hand, the standard deviation (SD) of the departures in Table 2 indicates that its values are only 1/3 to 1/6 of the annual departures over the ocean regions contrary to the very large SD over the land regions. Such a fact illuminates the stable departures between GPCP and TRMM PR over the ocean in contrast to the poignant and intricate departures over land.

Figure 5 demonstrates that the mean precipitation in each zone estimated by GPCP and TRMM PR shares the same seasonal cycling pattern. The figure also shows clear, opposite phase changes of precipitation between the two hemispheres, especially over land. Besides, the seasonal variability of precipitation over land is more significant than that over the ocean due to the remarkable, meridional shifts in the rainfall band. As for the departures between the two datasets, they do not show clear seasonal variability.

5. Effect of SSTA on departures of GPCP and TRMM PR

The 1997/1998 El Niño was the strongest one in the last century. The SST anomaly in the Niño 3 and 4 areas indicated that this El Niño event started in May 1997 and reached its mature phase at the end of 1997, then, it swiftly switched into a La Niña from May 1998.

In Fig. 6, the rainfall distributions over the tropical Pacific averaged from January to April in 1998 and the same period in 1999 are plotted, which represents respectively the latter phase of El Niño and La Niña by using GPCP (Figs. 6a and 6d) and TRMM PR (Figs. 6b and 6e). The rainfall differences between the two datasets in the same period are also plotted in Figs. 6c

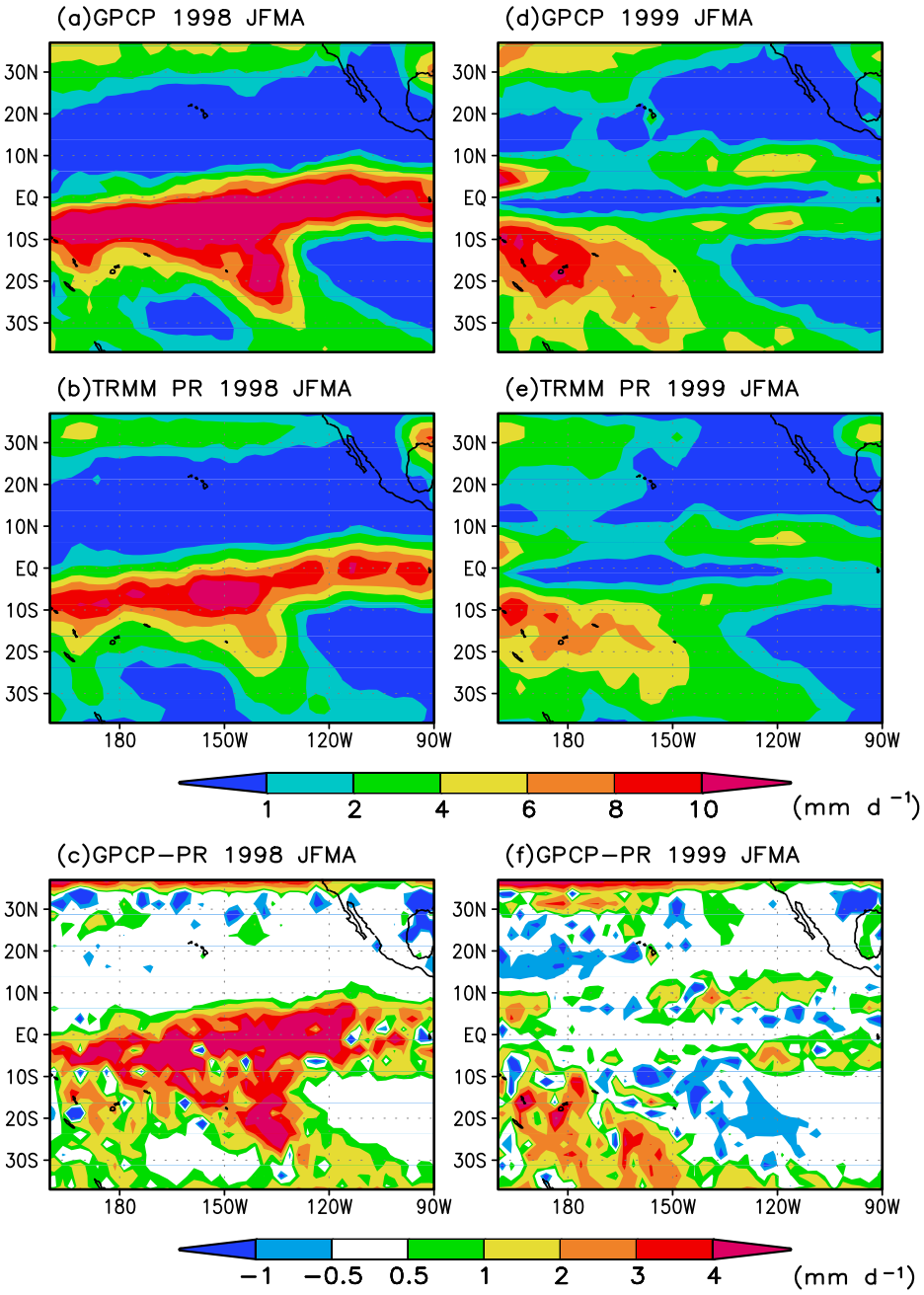

Fig. 6. The distribution of tropical Pacific precipitation estimated by GPCP and TRMM PR, and their difference (GPCP–PR) averaged from January to April 1998 (latter phase of El Niño) and the same period of 1999 (La Niña) (Units: mm d^{-1}).

and 6f. The rainfall pattern and vertical profile anomaly resulting from this El Niño have been studied by using TRMM PR measurements (Li et al., 2005). Here, rainfall differences produced by the SST anomaly in the latter phase of the 1997/1998 El Niño are emphasized in particular. It is very obvious that rainfall over the whole tropical ocean is greatly overestimated by GPCP than by TRMM PR during the latter phase of this El Niño (see Figs. 6a, 6b, and 6c), while in the same period of La Niña, the amplitude and area of the rainfall difference between both datasets are small (see Fig. 6f).

In our previous work (Li et al., 2005), the authors illustrated that the positive SSTA over the central and eastern Pacific Ocean in the latter phase of the 1997/1998 El Niño makes precipitation system deeper

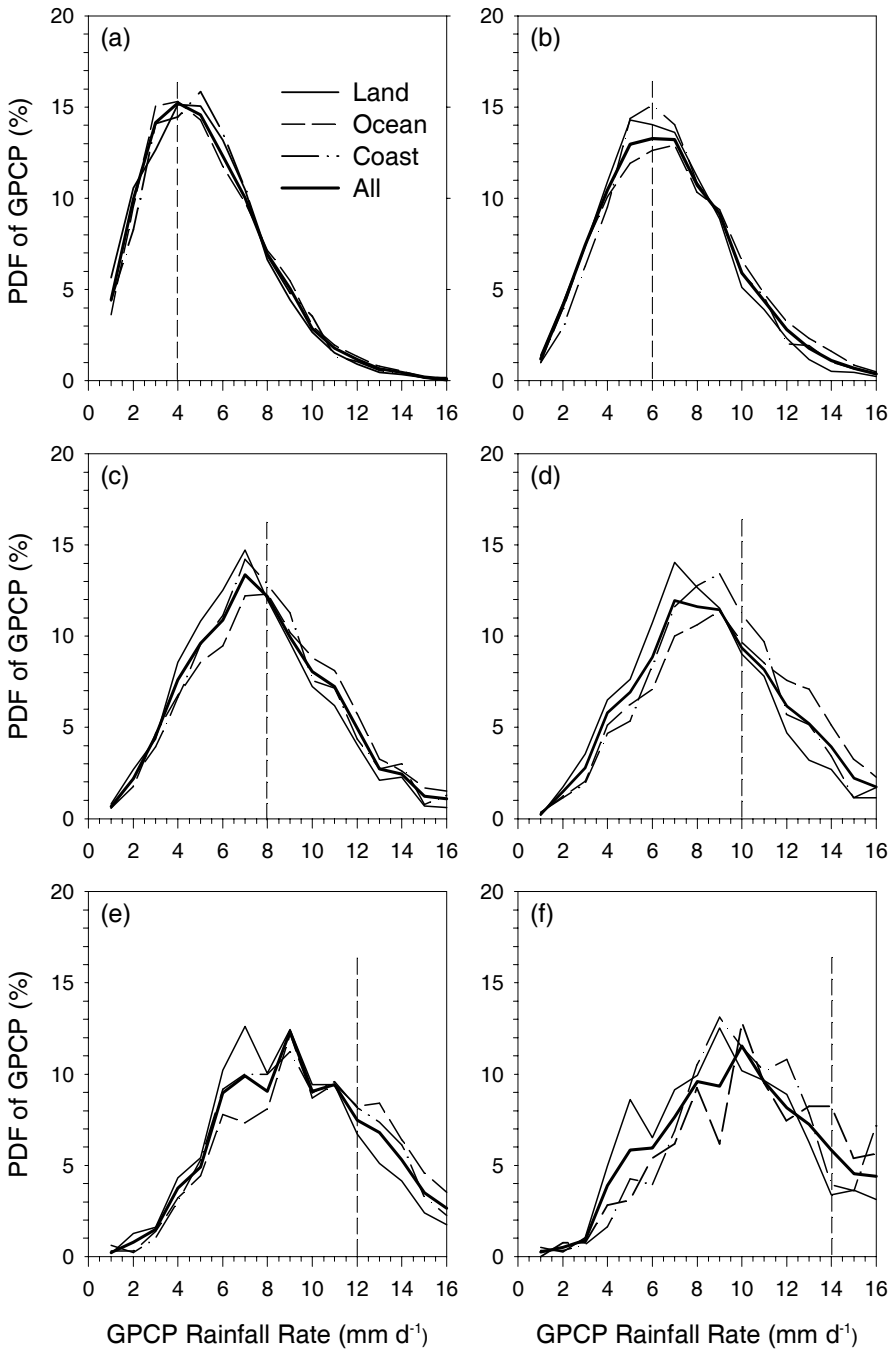

Fig. 7. GPCP PDF curves for a given rain rate estimated by TRMM PR in the range of (a) 3.5–4.5 mm d^{-1}, (b) 5.5–6.5 mm d^{-1}, (c) 7.5–8.5 mmd^{-1}, (d) 9.5–10.5 mm d^{-1}, (e) 11.5–12.5 mm d^{-1}, and (f) 13.5–14.5 mm d^{-1} over land, ocean, coast and all regions between 20°S and 20°N.

for convective rains and bright band uplifting for stratiform rains in that region. Results also indicate abnormal increases of the brightness temperatures at 10.7 GHz, 19.4 GHz and 22 GHz in TMI (TRMM Microwave Imager) for precipitating clouds over the central and eastern Pacific Ocean in the latter phase of the 1997/1998 El Niño contrary to normal SST over the regions. So, one needs to consider the effects of SSTA over the tropical Pacific Ocean on the rainfall retrieval algorithms from infrared (IR) temperatures

or microwave brightness temperatures.

6. Relationship of mean rainfall rate to the departure of GPCP and TRMM PR

To find out the relationship of rainfall estimates between GPCP and TRMM PR, first, the Probability Distribution Function (PDF) of GPCP estimates, which represents percentages of GPCP estimates by given TRMM PR estimates, is calculated in the region 20°S–20°N. Then, the departure variabilities of GPCP and TRMM PR estimates along with mean rainfall rates averaged by GPCP and TRMM PR estimates are analyzed.

Given a rainfall intensity estimate by TRMM PR, the PDF of the GPCP estimates is defined as:

$$PDF(i,j) = \frac{N(i,j)}{\sum_{j=1}^{J} N(i,j)} \times 100\% \, .$$

here, $N(i,j)$ is the number of samples when the rainfall intensity estimated by GPCP yields the interval of rainfall rate of $j-0.5, j+0.5$ together with the TRMM PR estimate in the interval of $i-0.5, i-+0.5$.

Figure 7 shows typical PDF curves varying over GPCP rain rates given rainfall intensity estimated by TRMM PR from 3.5 to 14.5 mm d^{-1} over land, ocean, coast, and all regions between 20°S and 20°N. It indicates that the GPCP PDF curves show a single peak pattern in these regions when the rain intensity estimated by TRMM PR is weaker than 12 mm d^{-1}. The maximum PDF of the GPCP samples is between 10% and 20%. When the rain intensity estimated by TRMM PR is weaker than 8 mm d^{-1}, the GPCP estimates corresponding to the maximum PDF are very close to the TRMM PR estimates in these regions. When rain intensity exceeds 8 mm d^{-1} but is still weaker than 12 mm d^{-1}, the GPCP estimates corresponding to the maximum PDF become obviously lower than those of TRMM PR. The profile differences among these regions also become larger. As the rain intensity exceeds 12 mm d^{-1}, the GPCP PDF curves show multiple peak patterns as well as a lower maximum PDF value due to enhancement of the sample scattering. Regional profiles fluctuate strongly and show obvious differences. The relationship between GPCP and TRMM PR estimates is not believeable when the rain intensity exceeds 16 mm d^{-1} because of the very serious sample scattering. The above illustrates a significant tendency of the departure distributions between GPCP and TRMM PR rainfall rate estimates, viz., both datasets have a better relationship when the rainfall rate is not very heavy. However, the GPCP rainfall rates become lower than the TRMM PR estimates usually as the rainfall rates increase.

Until now, there has not been an absolutely precise method to estimate rainfall distributions over the globe, as mentioned in the introduction. To better comprehend rainfall differences estimated by GPCP and TRMM PR, the rainfall rate departures between both estimates are contrasted with the mean rainfall rate averaged from both estimates in order to expose the bias between the GPCP and TRMM PR estimates at the given mean rainfall rate.

The mean rainfall intensity is calculated in each grid. Then, sample statistics are calculated over the land, ocean, coast, and globe (i.e., the combination of land, ocean and coast) for nine ranges of the mean rainfall rate, 0–2 mm d^{-1}, 2–4 mm d^{-1}, 4–6 mm d^{-1}, 6–8 mm d^{-1}, 8–10 mm d^{-1}, 10–12 mm d^{-1}, 12–14 mm d^{-1}, 14–16 mm d^{-1} and greater than 16 mm d^{-1}. Sample distributions in each range are shown in Fig. 8a, which shows that more than 40 percent are weak rainfalls regardless of surface type. About 50 percent of rainfalls occur with rainfall rates between 2 mm d^{-1} and 10 mm d^{-1}. Heavy rainfalls account for only less than 10 percent among all rainfall samples. Such sample distributions may reflect a universal law, i.e., heavy rainfall events are rare possibilities.

The relative and absolute departures between GPCP and TRMM PR estimates versus the mean rainfall rate are shown in Figs. 8b and 8c, respectively. It is obvious that over each kind of surface, the estimates of GPCP are higher than TRMM PR at weak and moderate rain intensity ranges but lower at a heavy rain rate. The value of the relative bias is the largest (>50%) at the weak rain intensity rate of 0–2 mm d^{-1}, especially over coastal regions, which indicates that there are uncertain estimates in both estimates in weak rainfalls. As the rain rate increases, the relative bias decreases from positive to negative. A small relative bias (less than 10 percent) occurs at rain rates between 7 mm d^{-1} and 11 mm d^{-1}. When the rain rate is greater than 11 mm d^{-1}, the relative bias also becomes large. Figure 8b also shows a significant difference in the relative bias over the ocean and the smallest bias over land at a given rain rate less than 12 mm d^{-1}, which is consistent with the discussion in section 4. However, when the given rain rate is greater than 12 mm d^{-1}, the opposite circumstance happens.

The absolute bias between GPCP and TRMM PR estimates for each kind of surface shown in Fig. 8c is less than 1 mm d^{-1} when the mean rain rate is less than 12 mm d^{-1} except for the ocean at a rain rate range between 7 mm d^{-1} and 11 mm d^{-1}. However, the bias increases rapidly as the rain rate increases,

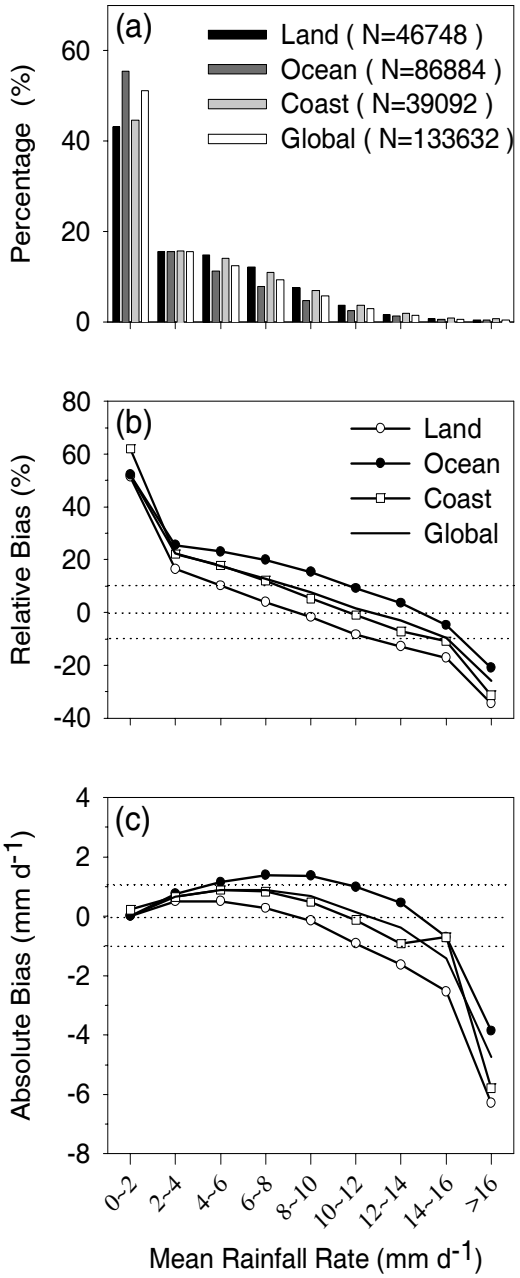

Fig. 8. (a) Sample distributions in nine rainfall rate ranges, (b) curves of relative bias and (c) absolute bias between GPCP and TRMM PR estimates versus the mean rainfall rate over the land, ocean, coast, and globe.

especially for a rain rate greater than 15 mm d^{-1} for the bias over land, which implies that the rainfall retrieval algorithm requires further development for cases of heavy precipitating clouds.

Because the sensitivity of TRMM PR is about 17 dBZ, it cannot accurately detect very weak rain (weaker than 0.4 mm h^{-1}). This may be the main reason for the larger relative bias between GPCP and TRMM PR estimates in the very weak rain intensity range. In this case, the estimates of GPCP may be viewed as more credible. On the other hand, the microwave emission signals are saturated at higher rain intensity so that an emission-based algorithm, such as SSM/I E, cannot be performed well for estimating heavy rain. This may indicate why there are large biases between GPCP and TRMM PR in estimating heavy rain. Possibly, TRMM PR estimates heavy rain more accurately if the TRMM PR echo extenuation is not serious.

7. Conclusion

In this study, rainfall differences derived from GPCP and TRMM PR estimates over the Tropics on the monthly scale are compared in the period from 1998 to 2002 in order to illuminate uncertainties in both rainfall datasets and their reasons. The relations between the differences and the precipitation intensity are presented as a reference for future cross correction of both datasets.

First, the mean statuses of both estimates averaged over the period from 1998 to 2002 are compared, which shows that both datasets are consistent in depicting the horizontal distribution pattern of the tropical monthly mean precipitation. However, significant differences exist in the regions with heavy precipitation zones in the tropical oceans as well as in their vicinity. Usually, the mean precipitation estimate by GPCP is higher than that of TRMM PR over the tropical oceans, about 0.45 mm d^{-1} on average, which results mainly from the estimate differences between passive emission microwave retrievals (SSM/I E) and active microwave measurement (TRMM PR). Over land, the mean difference between GPCP and TRMM PR estimates is about 0.08 mm d^{-1}. However, detailed differences over land are largely correlated with the distribution density of GPCC rain gauge stations. In regions where rain gauge stations are rare or sparse, GPCP tends to underestimate the precipitation in the region, whereas in the regions densely covered by GPCC stations, TRMM PR estimates of precipitation are smaller than the real observations of the gauges.

The temporal variability of the difference between GPCP and TRMM PR estimates shows the agreement of both on the seasonal cycle of the tropical precipitation. However, it reveals the positive departure of GPCP from TRMM PR over the ocean regardless of season, i.e., departures over the ocean show less seasonal variability. The maximum departure of both datasets, about 0.8 mm d^{-1} in the annual mean, over the ocean appears in the zone from 0° to 15°N in the four seasons. In the other zones, the annual departures are less than 0.5 mm d^{-1}. Over land, the seasonal departures of the two datasets show relatively strong

seasonal variability, which results in less than 0.4 mm d^{-1} in annual mean departure. This implies a better retrieval of precipitation by GPCP over land than over the ocean. On the other hand, the standard deviation (SD) of the departures take values of only 1/3 to 1/6 in the annual scale over oceanic regions contrary to the very large SDs over land regions, which illuminates the stable departures between GPCP and TRMM PR over the ocean in contrast with the poignant and intricate departures over land.

Rainfall differences produced by the SST anomaly in the latter phase of the 1997/1998 El Niño are analyzed. Results show that rainfall over the whole tropical ocean is greatly overestimated by GPCP than by TRMM PR during the latter phase of this El Niño. While in the same period of La Niña, the amplitude and area of the rainfall difference between the two datasets become small.

Lastly, relationships of the bias between GPCP and PR versus precipitation intensity are investigated. For a given rain intensity estimated by TRMM PR, the PDFs of the GPCP estimates show a single-peak pattern when the mean rain rate is less than 12 mm d^{-1}, but a multiple-peak pattern occurs as the mean rain rate increases. When the rain intensity exceeds 8 mm d^{-1} but remains weaker than 12 mm d^{-1}, the GPCP estimates corresponding to the maximum PDF become obviously lower than those of TRMM PR. Because of such a serious sample scattering, the relationship between GPCP and TRMM PR estimates are not believable when the rain intensity exceeds 16 mm d^{-1}. This result illustrates the relatively better relationship between the two datasets when the rainfall rate is not very heavy. However, GPCP estimates usually become lower than the TRMM PR estimates as the rainfall rates increase.

The variation of the relative and absolute departures between GPCP and TRMM PR estimates with the mean rainfall rate shows that the estimates of GPCP are higher than TRMM PR in weak and moderate rain intensity ranges but lower at a heavy rain rate. The value of the relative bias becomes largest (>50%) at the weak rain intensity of 0–2 mm d^{-1}, especially over coastal regions. A small relative bias (less than 10 percent) occurs at a rain rate between 7 mm d^{-1} and 11 mm d^{-1}. The results also show a significant difference in the relative bias over the ocean and the smallest difference over land at a given rain rate less than 12 mm d^{-1}. However, when the given rain rate is greater than 12 mm d^{-1}, the opposite circumstance happens. The absolute bias between the GPCP and TRMM PR estimates is less than 1 mm d^{-1} when the mean rain rate is less than 12 mm d^{-1} except for the ocean at a rain rate range between 7 mm d^{-1} and 11 mm d^{-1}. However, the bias increases rapidly as the rain rate increases especially for a rain rate greater than 15 mm d^{-1} for the bias over land, which implies that the rainfall retrieval algorithm requires further developmant for cases of heavy precipitating clouds.

Acknowledgments. This research has been supported by NKBRDPC Grant No. 2004CB418304, NSFC Grant Nos. 40175015 and 40375018 and NSFC grant of the Joint Research Fund for Overseas Chinese Young Scholars (No. 40428006), EORC/JAXA (No. 206).

REFERENCES

Adler, R. F., G. J. Huffman, D. T. Bolvin, S. Curtis, and E. J. Nelkin, 2000: Tropical rainfall distribution determined using TRMM combined with other satellite and rain gauge information. *J. Appl. Meteor.*, **39**, 2007–2023.

Adler, R. F., C. Kidd, G. Petty, M. Morissey, and H. M. Goodman, 2001: Intercomparison of global precipitation products: The Third Precipitation Intercomparison Project (PIP-3). *Bull. Amer. Meteor. Soc.*, **82**, 1377–1396.

Adler, R. F., and Coauthors, 2003: The Version-2 Global Precipitation Climatology Project (GPCP) monthly precipitation analysis (1979–present). *Journal of Hydrometerology*, **4**, 1147–1167.

Arkin, P. A., and B. N. Meisner, 1987: The relationship between large-scale convective rainfall and cold cloud over the Western Hemisphere during 1982–84. *Mon. Wea. Rev.*, **115**, 51–74.

Awaka, J., T. Iguchi, and K. Okamoto, 1998: Early results on rain type classification by the Tropical Rainfall Measuring Mission (TRMM) precipitation radar. Proceedings of 8th URSI Commission F Open Symp., Averior, Portugal, 134–146.

Bartter, E. C., and Coauthors, 1994: The first WETNET precipitation intercomparison project: Interpretation of results. *Remote Sensing Reviews*, **11**, 303–373.

Berg, W., C. Kummerow, and C. A. Morales, 2002: Differences between East and West Pacific rainfall systems. *J. Climate*, **15**, 3659–3672.

Cruber, A., X. J. Su, M. Kanamitsu, and J. Schemm, 2000: The comparison of two merged rain gauge-satellite precipitation datasets. *Bull. Amer. Meteor. Soc.*, **81**, 2631–2644.

Ebert, E. E., 1996: Results of the 3rd Algorithm Intercomparison Project (AIP-3) of the Global Precipitation Climatology Project (GPCP), Revision 1. Bureau of Meteorology Research Center, 199pp.

Ferrraro, R., and G. Marks, 1995: The development of SSM/I rainrate retrieval algorithm using ground-based radar measurements. *J. Atmos. Oceanic. Technol.*, **12**, 755–770.

Ferraro, R., F. Weng, N. C. Grody, and A. Basist, 1996: An eight-year (1987–1994) time series of rainfall, clouds, water vapor, snow cover, and sea ice derived from SSM/I measurements. *Bull. Amer. Meteor. Soc.*, **77**, 891–905.

Fu, Y., and G. Liu. 2001: The variability of tropical precipitation profiles and its impact on microwave brightness temperatures as inferred from TRMM data. *J. Appl. Meteor.*, **40**, 2130–2143.

Fu, Y., and G. Liu, 2003: Precipitation characteristics in mid-latitude East Asia as observed by TRMM PR and TMI. *J. Meteor. Soc. Japan*, **81**, 1351–1367.

Fu, Y., Y. H. Lin, G. Liu, and Q. Wang. 2003a: Seasonal characteristics of precipitation in 1998 over East Asia as derived from TRMM PR. *Adv. Atmos. Sci.*, **20**, 511–529.

Fu, Y., R. Yu, Y. Xu, Q. Xiao, and G. Liu, 2003b: Analysis on precipitation structures of two heavy rain cases by using TRMM PR and TMI. *Acta Meteor. Sinica*, **61**, 421–431. (in Chinese)

Grody, N. C., 1991: Classification of snow cover and precipitation using the Special Sensor Microwave/Imager (SSM/I). *J. Geophys. Res.*, **96**, 7423–7435.

Gruber, A., X. J. Su, M. Kanamitsu, and J. Schemm, 2000: The comparison of two merged rain gauge-satellite precipitation datasets. *Bull. Amer. Meteor. Soc.*, **81**, 2631–2644.

Haddad, Z. S., E. A. Smith, C. D. Kummerow, T. Iguchi, M. R. Farrar, S. L. Durden, M. Alves, and W. S. Olson, 1997: The TRMM "Day-1" radar/radiometer combined rain-profiling algorithm. *J. Meteor. Soc. Japan*, **75**, 799–809.

Halpern, D., and C. W. Hung, 2001: Satellite observations of the Southeast Pacific intertropical convergence zone during 1993–1998. *J. Geophys. Res.*, **106**(22), 28107–28112.

Huffman, G. J., and Coauthors, 1997: The Global Precipitation Climatology Project (GPCP) Combined Precipitation Dataset. *Bull. Amer. Meteor. Soc.*, **78**, 5–20.

Iguchi, Toshio, and Robert Meneghini, 1994: Intercomparison of single-frequency methods for retrieving a vertical rain profile from airborne or space radar data. *J. Atmos. Oceanic Technol.*, **11**, 1507–1516.

Kummerow, C., W. Barnes, T. Kozu, J. Shiue, and J. Simpson, 1998: The Tropical Rainfall Measuring Mission (TRMM) sensor package. *J. Atmos. Oceanic Technol.*, **15**, 809–817.

Kummerow, C., and Coauthors, 2000: The status of the Tropical Rainfall Measuring Mission (TRMM) after two years in orbit. *J. Appl. Meteor.*, 1965–1982.

Kummerow, C., and Coauthors, 2001: The evolution of the Goddard Profiling Algorithm (GPROF) for rainfall estimation from passive microwave sensors. *J. Appl. Meteor.*, **40**, 1801–1820.

Kummerow, C., P. Poyner, W. Berg, and J. Thomas-Stahle, 2004: The effects of rainfall inhomogeneity on climate variability of rainfall estimated from passive microwave sensors. *J. Atmos. Oceanic Technol.*, **21**, 624–638.

Li Rui, Fu Yunfei, and Zhao Ping, 2005: Characteristics of rainfall structure over the tropical Pacific during the later period of 1997/1998 El Nino derived from TRMM PR observations. *Chinese J. Atmos. Sci.*, **29**, 225–234.

Liu, G., and Y. Fu, 2001: The characteristics of tropical precipitation profiles as inferred from satellite radar measurements. *J. Meteor. Soc. Japan*, **79**, 131–143.

Masunaga, H., T. Iguchi, R. Oki, and M. Kachi, 2002: Comparison of rainfall products derived from TRMM Microwave Imager and Precipitation Radar. *J. Appl. Meteor.*, **41**, 849–862.

New, M., M. Todd, and P. Jones, 2001: Precipitation measurements and trends in the twentieth century. *Int. J. Climatol.*, **21**, 1899–1922.

Petersen, W. A., and S. A. Rutledge, 2001: Regional variability in tropical convection: Observations from TRMM. *J. Climate*, **14**, 3566–3585.

Rudolf, B., 1993: Management and analysis of precipitation on a routine basis. *Proc. Int. WMO/IAHS/ETH/SYMP.* On Precipitation and Evaporation, Slovak Hydrometeorology Institute, Bratislava, 69–76.

Rudolf, B., H. Hauschild, W. Rueth and U. Schneider, 1994: Terrestrial precipitation analysis: Operational method and required density of point measurements. *Global Precipitations and Climate Change*, M. Desbois and F. Desalmond, Eds., NATO ASI Series I, **26**, Springer-Verlag, 173–186.

Rudolf, B., T. Fuchs, U. Schneider, and A. Meyer-Christoffer, 2003: Introduction of the Global Precipitation Climatology Centre (GPCC), Deutscher Wetterdienst, Offenbach a.M., 16pp. [available on request per email gpcc@dwd.de].

Shin, D-B, L. S. Chiu, and M. Kafatos, 2001: Comparison of the monthly precipitation derived from TRMM satellite. *Geophys. Res. Lett.*, **28**, 795–798,

Simpson, J., R. F. Adler, and G. R. North, 1988: A proposed Tropical Rainfall Measuring Mission (TRMM) satellite. *Bull. Amer. Meteor. Soc.*, **69**, 278–295

Smith, E. A., and Coauthors, 1998: Results of WetNet PIP-2 Project. *J. Atmos. Sci.*, **55**, 1483–1536.

Soden, B. J., 2000: The sensitivity of the tropical hydrological cycle to ENSO. *J. Climate.*, **13**, 538–549.

Sussikind, J., P. Piraino, and L. Rokke, *T. Iredell, and A. Mehta*, 1997: Characteristics of the TOVS pathfinder path A dataset. *Bull. Amer. Meteor. Soc.*, **78**, 1449–1472.

Weng, F., and N. C. Grody, 1994: Retrieval of cloud liquid water using the Special Sensor Microwave Imager (SSM/I). *J. Geophys. Res.*, **99**, 25535–25551.

Wilheit, T. J., A. T. C. Chang, and L. S. Chiu, 1991: Retrieval of monthly rainfall indices from microwave radiometric measurements using probability distribution functions. *J. Atmos. Oceanic Technol.*, **8**, 118–136.

Xie, P. P., and P. A. Arkin, 1996: Analysis of global monthly precipitation using gauge observation, satellite estimates, and numerical model predictions. *J. Climate*, **9**, 840–858.

Xie, P. P., and P. A. Arkin, 1997: Global Precipitation: A 17-year monthly analysis based on gauge observation, satellite estimates, and numerical model outputs. *Bull. Amer. Meteor. Soc.*, **78**, 2539–2558.

Xie, P. P., and P. A. Arkin, 1998: Global monthly precipitation estimates from satellite-observed outgoing longwave radiation. *J. Climate*, **11**, 137–164.

Zheng Yuanyuan, Fu Yunfei, Liu Yong, Zhu Hongfei, Xie Yifeng, Yao Xiuping, and Yu Rucong, 2004: Heavy rainfall structures and lightning activities in a cold front cyclone happened in Huai river derived from TRMM PR and LIS observations. *Acta Meteorologica Sinica*, **62**, 790–802.